Onset of wavy vortices in the finite-length Couette–Taylor problem

W. S. Edwards,[a] S. R. Beane,[b] and S. Varma[b]
Center for Nonlinear Dynamics and Department of Physics, University of Texas at Austin, Austin, Texas 78712

(Received 22 October 1990; accepted 19 February 1991)

The transition from Taylor vortex flow to wavy vortex flow in the Couette–Taylor problem, for finite annulus lengths, is studied. Using an accurate, fully resolved numerical code, infinite-cylinder nonlinear axisymmetric Taylor vortices are computed and their stability with respect to nonaxisymmetric disturbances corresponding to wavy vortices is determined. The present method computes leading eigenmodes and eigenvalues for arbitrary axial Floquet exponents k and arbitrary azimuthal wave numbers m, so that the full complex dispersion relation $\omega = \omega(k,m)$ is obtained. The linear coefficients appearing in the Ginzburg–Landau equation are calculated and compared to previous experimental results. It is found that for aspect ratios (length to gap width) less than 30, the Ginzburg–Landau predictions are not reliable; for these aspect ratios the transition is modeled as the superposition of two Floquet modes with $k = \pm \pi/L$, where L is the length of the annulus. This model is verified via a detailed numerical and experimental study at aspect ratios between 8 and 34, for radius ratio 0.87, obtaining good agreement for the critical Reynolds numbers, azimuthal wave numbers and wave speeds over the entire aspect-ratio range.

I. INTRODUCTION

The instabilities arising the Couette–Taylor problem have been well studied since the classic work of Taylor.[1] With the outer cylinder fixed and inner cylinder rotating, the primary transition from circular Couette flow to Taylor vortices is predicted well by linear theory in the infinite-cylinder approximation. The observed secondary transition to wavy vortices is also in rough agreement with linear calculations,[2-4] although it is well known that the finite length of the annulus strongly influences the observed critical Reynolds number and azimuthal wave number.[2,5] The problem has been analyzed with the help of a Ginzburg–Landau equation[6,7] with coefficients obtained from experimental data.

Jones[3,4] has numerically computed critical linear modes for wavy vortices in the infinite-cylinder approximation. His calculations were limited to modes with the same wavelength as the underlying Taylor vortex flow. Our numerical study is in the same spirit; that is, we calculate fully nonlinear axisymmetric Taylor vortices at a given Reynolds number R, and we linearize around this flow. However, we go beyond the assumption of axially periodic disturbances by considering modes with arbitrary Floquet exponent k in the axial direction. While it is true that the critical wavy vortex disturbance in the infinite-cylinder approximation is always found to be periodic, that is, to have $k = 0$, the ability to vary k allows the computation of linear coefficients of the Ginzburg–Landau equation. In addition, we have successfully modeled the transition in cylinders of finite length L by assuming that only two Floquet modes, with $k = \pm \pi/L$, are sufficient to account for it. Direct computation of these modes and their critical Reynolds numbers and wave speeds takes us beyond the Ginzburg–Landau approximation of a quadratic dispersion relation. We obtain accurate predictions for annulus lengths as short as $L = 4\lambda_c \approx 8$, where λ_c is the wavelength of the critical Taylor vortex mode.

The following sections state the problem and set out our notation, describe our numerical methods, give numerical results for linear Ginzburg–Landau coefficients corresponding to previously published experimental work, describe our two-Floquet-mode model and our detailed numerical and experimental aspect-ratio study, and compare numerical and experimental results. A brief concluding section suggests an extension of the model to the nonlinear case.

II. PROBLEM STATEMENT

A. Geometry and dimensionless parameters

Figure 1 shows the geometry and coordinate system. The flow of a Newtonian fluid of kinematic viscosity ν takes place in the annular region between cylinders of length L and of radii a and b with $b > a$. The outer cylinder is at rest and the inner cylinder rotates with angular speed Ω. We define three dimensionless parameters (η,Γ,R), which are the radius ratio $\eta = a/b$, the aspect ratio $\Gamma = L/(b-a)$, and the Reynolds number $R = \Omega a(b-a)/\nu$. Transition from Couette flow to Taylor vortices is brought about by increasing R while keeping η and Γ fixed; the critical Reynolds number for infinite-cylinder transition to Taylor vortices, denoted R_c is a strong function of η.

B. Navier–Stokes equations, Couette flow, and Taylor vortices

The Navier–Stokes equations in coordinate-free notation are

[a] Present address: Laboratoire de Physique, Ecole Normale Supérieure de Lyon, 46 allée d'Italie, 69364 Lyon Cedex 07, France.
[b] Present address: Center for Particle Theory, University of Texas, Austin, Texas 78712.

 0899-8213/91/061510-09$02.00

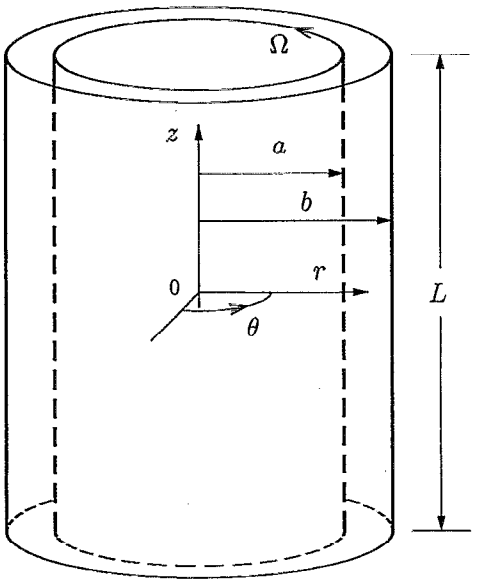

FIG. 1. Geometry and coordinate system.

$$\partial_t \mathbf{U} = -(\mathbf{U}\cdot\nabla)\mathbf{U} + \nu\nabla^2\mathbf{U} - \nabla P, \tag{1}$$

$$\nabla\cdot\mathbf{U} = 0, \tag{2}$$

where we have chosen units of mass such that the fluid density is identically 1. We use cylindrical coordinates (r,θ,z) with velocity components (U_r,U_θ,U_z). The no-slip conditions at the inner and outer cylinder walls are

$$\mathbf{U} = \Omega a\mathbf{e}_\theta, \quad \text{at } r = a, \tag{3}$$

$$\mathbf{U} = \mathbf{0}, \quad \text{at } r = b, \tag{4}$$

where $\mathbf{e}_\theta$ is the azimuthal unit vector. The circular Couette flow solution to (1,2,3,4) for infinitely long cylinders is

$$\mathbf{U}_C = (Ar + B/r)\mathbf{e}_\theta, \tag{5}$$

where the constants A and B are chosen to satisfy the no-slip conditions (3) and (4) and have the values $A = -\Omega a^2/(b^2-a^2)$, $B = \Omega a^2 b^2/(b^2-a^2)$. The associated pressure field is

$$P_C(r) = \int dr \frac{|\mathbf{U}_C|^2}{r} = \frac{A^2 r^2}{2} + 2AB\ln r - \frac{B^2}{2r^2}. \tag{6}$$

The field $\mathbf{U}_C$ has all the symmetries of the equations and boundary conditions. Explicitly, these are the three continuous symmetries:

$$\text{translational invariance:} \quad \partial_z \mathbf{U}_C = \mathbf{0}, \tag{7}$$

$$\text{axisymmetry:} \quad \partial_\theta \mathbf{U}_C = \mathbf{0}, \tag{8}$$

$$\text{steady state:} \quad \partial_t \mathbf{U}_C = \mathbf{0}, \tag{9}$$

and the discrete reflection symmetry in z:

$$S_z\mathbf{U}_C = \mathbf{U}_C, \tag{10}$$

where the reflection operation S_z is defined by

$$S_z\mathbf{U}(r,\theta,z,t) = [U_r(r,\theta,-z,t), U_\theta(r,\theta,-z,t), -U_z(r,\theta,-z,t)]. \tag{11}$$

There exists a critical Reynolds number $R_c = R_c(\eta)$ such that Couette flow is stable only for $R < R_c$. At $R = R_c$ there is a neutrally stable eigenmode associated with the transition to Taylor vortices. This mode is axisymmetric and has one Fourier component in the axial direction with wavelength λ_c. All other Fourier modes and nonaxisymmetric modes are damped. The transition to Taylor vortices is a supercritical bifurcation, and just beyond R_c a pattern of toroidal vortices develops with approximately the wavelength λ_c. In experiments the actual wavelength observed for nonlinear Taylor vortices depends on the length L of the apparatus and also on the experimental protocol; we will return to this issue when we discuss our experimental study.

The Taylor vortex velocity field $\mathbf{U}_T$, with pressure P_T, breaks the axial translational invariance of Couette flow. It is steady state and axisymmetric and reflection symmetric about vortex boundaries. There are two vortices per axial wavelength, and adjacent vortices are separated by *inflow* or *outflow* boundaries along which the flow is radially inward or outward, respectively. Taylor vortices are periodic in the z direction, which we express by the notation

$$\exp(\lambda_c\partial_z)\mathbf{U}_T = \mathbf{U}_T, \tag{12}$$

where the operator $\exp(\lambda_c\partial_z)$ is an axial translation by λ_c.

C. Linearization

The linear stability problem for the transition to wavy vortices is obtained by substituting $\mathbf{U}\to\mathbf{U}_T+\mathbf{u}$ and $P\to P_T+p$ into (1) and (2) and retaining only terms linear in the perturbation variables $\mathbf{u}$ and p. This yields

$$\partial_t\mathbf{u} = -(\mathbf{U}_T\cdot\nabla)\mathbf{u} - (\mathbf{u}\cdot\nabla)\mathbf{U}_T + \nu\nabla^2\mathbf{u} - \nabla p, \tag{13}$$

$$\nabla\cdot\mathbf{u} = 0 \tag{14}$$

No-slip conditions (3) and (4) for the total field imply, for the perturbation,

$$\mathbf{u} = \mathbf{0}, \quad \text{at } r = a,b. \tag{15}$$

The symmetries of the Taylor vortex flow allow us to seek eigenmodes of the form

$$\mathbf{u}(r,\theta,z,t) = \hat{\mathbf{u}}(r,z \bmod \lambda_c)e^{im\theta + ikz - i\omega t} + \text{c.c.}, \tag{16}$$

where the azimuthal wave number m is restricted to be integer by the requirement that the flow be periodic in θ, and ω is complex with $\mathrm{Im}(\omega)$ being the growth rate. The azimuthal wave speed of the mode is given by $\mathrm{Re}(\omega)/m$. The Floquet parameter k is taken to be real and without loss of generality we may consider only k's within the first Brillouin zone defined by $-\pi/\lambda_c \leqslant k \leqslant +\pi/\lambda_c$.

Numerical calculation of the nonlinear Taylor vortex flow and solution of the linear stability eigenproblem is performed by an accurate and efficient spectral method that will be described in a future publication.[8] Here we note only that the computations are performed on a small two-dimensional (r,z) domain, periodic in z with period λ_c, and that this is true of both the Taylor vortex nonlinear computations and the solution of the eigenproblem. These computations allow full investigation of the complex dispersion relation $\omega = \omega(m,k;R,\eta,\lambda_c)$.

III. FINITE ASPECT RATIO: GINZBURG–LANDAU EQUATIONS

A. Linear coefficients and the dispersion relation

Experimental evidence (Ref. 7 and references cited therein) suggests that the dynamics of wavy vortices near transition may be modeled by the one-dimensional complex Ginzburg–Landau equation

$$\tau_0 \partial_t A = \epsilon(1 + ic_0)A + \xi_0^2(1 + ic_1)\partial_z^2 A - g|A|^2 A, \tag{17}$$

where $\epsilon = (R - R_W)/R_W$, with R_W being the critical Reynolds number for onset of waves in the infinite-cylinder case. The complex amplitude $A = A(z,t)$ is assumed to be slowly varying in both z and t, such that the disturbance velocity field is approximated by

$$\mathbf{u} \approx A(z,t)\hat{\mathbf{u}}(r, z \bmod \lambda_c)\exp(im_W\theta - i\omega_W t) + \text{c.c.} \tag{18}$$

Here $\hat{\mathbf{u}}(r, z \bmod \lambda_c)\exp(im_W\theta - i\omega_W t)$ is the critical infinite-cylinder wavy-vortex eigenmode with $k_W = 0$. We assume that in (17) the nonlinear coefficient g has positive real part so that the bifurcation is supercritical. The linear coefficients are obtained from the dispersion relation via the Taylor series approximation

$$\omega(m,k;\epsilon) - \omega|_W \approx \epsilon(\partial_\epsilon \omega|_W) + \tfrac{1}{2}k^2(\partial_k^2 \omega|_W). \tag{19}$$

Substituting $A = \exp[ikz - i(\omega - \omega_W)t]$ into (17), ignoring the nonlinear term, evaluating ∂_t and ∂_z^2 and equating coefficients of ϵ and k^2 between the resulting equation and (19) leads to the following explicit expressions for computing τ_0, c_0, ξ_0^2 and c_1 from $\omega(m,k;\epsilon)$:

$$\tau_0 = [\operatorname{Im}(\partial_\epsilon \omega|_W)]^{-1}, \tag{20}$$

$$c_0 = -\tau_0 \operatorname{Re}(\partial_\epsilon \omega|_W), \tag{21}$$

$$\xi_0^2 = -(\tau_0/2)\operatorname{Im}(\partial_k^2 \omega|_W), \tag{22}$$

$$c_1 = (\tau_0/2\xi_0^2)\operatorname{Re}(\partial_k^2 \omega|_W). \tag{23}$$

We evaluate these derivatives at criticality ($\epsilon = 0, k = 0$) by finite differencing in ϵ (for τ_0 and c_0) and k (for ξ_0^2 and c_1).

B. Threshold and frequency shifts

A simple consequence of (17) is a shift in the critical Reynolds number for onset of wavy vortices in a system of finite length L relative to that for infinitely long cylinders. Assuming boundary conditions $A(\pm L/2,t) = 0$, and substituting $\partial_t \to -i\omega_L$ with ω_L real, the *first* eigenmode of the linearization of (17), that is, the eigenmode with smallest $\epsilon = \epsilon_L$, is

$$A_L(z,t) = \cos(\pi z/L)\exp(-i\omega_L t). \tag{24}$$

Substituting this in (17), evaluating the derivatives and dividing through by $A(z,t)$ produces the relation

$$-i\tau_0\omega_L = \epsilon_L(1 + ic_0) - \xi_0^2(1 + ic_1)(\pi^2/L^2). \tag{25}$$

The real part of this equation yields the threshold shift

$$\epsilon_L = \pi^2\xi_0^2/L^2 \tag{26}$$

and the imaginary part, with (26) gives the frequency shift

$$\omega_L = \tau_0^{-1}[\pi^2\xi_0^2(c_1 - c_0)/L^2]. \tag{27}$$

The $1/L^2$ correction (26) to the critical Reynolds number is in good agreement with experiments[5] in a long-aspect-ratio system ($\Gamma \geqslant 30$) of radius ratio $\eta = 0.89$, when the values $\xi_0 = 2.6$ and $R_W = 1.090R_c$ are used to fit the data. We note, however, that each azimuthal wave number m has its own infinite-cylinder critical R_W, its own values of the linear coefficients, and thus its own threshold and frequency shifts. The critical azimuthal wave number for annulus length L is the one whose shifted R_W is least at that L. The experimental data cited included observations of $m_W = 2$, 3, 4 and thus provide a good test of these threshold-shift predictions. However, the analysis of Ahlers[7] assumed that the various azimuthal wave numbers had similar infinite-cylinder R_W's and ξ_0's, and thus only one value for R_W and one value for ξ_0 were determined from the data. Our numerical calculations for this radius ratio are shown in Table I and Fig. 2. We do not find that $m_W = 4$ is predicted by Ginzburg–Landau threshold shifts in the range of aspect ratios reported, so its appearance in the experimental results is anomalous from this point of view. In Sec. IV we will propose a model which appears to accurately predict R_W, m_W, and ω_W over a wide range of aspect ratios.

The fact that azimuthal wave numbers other than 1 are observed at onset of wavy vortices is due to the finite length of the annulus. We note that the analysis of Walgraef *et al.*[9] predicts that higher azimuthal wave numbers will be observed at lower aspect ratios.

To our knowledge experimental results for the frequency correction (27) have not been previously reported.

C. Extrapolation to infinite aspect ratio

Pfister and Rehberg[6] noted that the stationary nonlinear equation (17) with $c_0 = c_1 = 0$ may be integrated using Jacobi elliptic functions; this result was fitted to experimental measurements of $|A(z)|$ for various values of R above R_W. The procedure allowed ϵ to be determined from R, from which extrapolation to $\epsilon = 0$ yielded R_W for the infinite-cylinder problem. This provides us with a good experimental case against which to test our numerical code with $k = 0$. Their experimental radius ratio was $\eta = 0.5066$, for which they found $R_W = 455$ for $m = 1$. The annulus length was

TABLE I. Numerical results for radius ratio $\eta = 0.89$ corresponding to experiments of Dominguez-Lerma *et al.*[5] Onset of Taylor vortices occurs at $R_c = 125.67$ with $\lambda_c = 2.0080(b - a)$. Here R_W refers to the critical Reynolds number for the onset of waves for infinite cylinders, τ_0 and ξ_0 are as in (20) and (22). The column $\xi_0\sqrt{R_W/R_c}$ is shown for comparison with Fig. 22 of Ahlers,[7] which defines ξ_0 differently from our convention. The values reported in that paper were $R_W/R_c = 1.09$ and $\xi_0\sqrt{R_W/R_c} = 2.7$, which were assumed to be approximately independent of m. The value $\pi^2\xi_0^2$ is the coefficient of the $1/L^2$ threshold shift (26). See also Fig. 2.

m	R_W/R_c	τ_0	ξ_0	$\xi_0\sqrt{R_W/R_c}$	$\pi^2\xi_0^2$
1	1.080	0.553	4.9	4.7	237
2	1.089	0.159	2.60	2.72	66.7
3	1.104	0.085	1.88	1.98	34.9
4	1.127	0.058	1.55	1.64	23.7

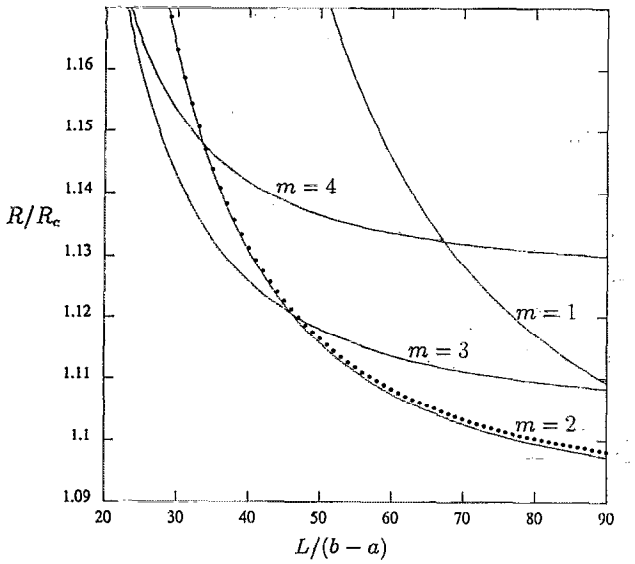

FIG. 2. Comparison of calculated Ginzburg–Landau threshold shifts with previous experimental results. Solid curves represent thresholds predicted from the first eigenmode of the G-L equation using the coefficients shown in Table I. The dotted line is the fit to the experimental data of Dominguez-Lerma *et al.*,[5,7] which included $m = 2,3,4$. It agrees well with our $m = 2$ neutral curve, but there is no obvious reason for the agreement. However, the experimentally observed $m = 4$ results do not agree with the G–L threshold shifts in this range of aspect ratios.

$18.5(b-a)$ and their base Taylor vortex flow had nine pairs of vortices, for an average wavelength of $2.056(b-a)$. Using this wavelength and radius ratio we find $R_W = 445$. The 2.2% discrepancy between the critical Reynolds numbers may be due to end effects in the experiments, the approximations inherent in the Ginzburg–Landau analysis including the assumption $c_0 = c_1 = 0$, or errors introduced in fitting the data to the Jacobi elliptic functions and extrapolating; no error analysis was presented in their paper. Another possible explanation is that at these aspect ratios there exist distinct modes with similar critical Reynolds numbers; our computed critical eigenmode's largest amplitude was on the outflow boundary, which agrees with descriptions of the so-called "jet-flow" mode.

IV. FLOQUET THEORY FOR THE ASPECT-RATIO DEPENDENCE OF THE ONSET OF WAVY VORTICES

A. Floquet modes and the axisymmetric end boundaries

The simple cosine eigenmode (24) of the linear Ginzburg–Landau equation may be rewritten trivially as

$$\cos(\pi z/L) = \tfrac{1}{2}(e^{ikz} + e^{-ikz}), \tag{28}$$

where $k = \pi/L$. This suggests that the linear eigenmode of the finite-length problem may be viewed as the superposition of two eigenmodes of the form (16) with $k = \pm \pi/L$. The advantage of this viewpoint is that it avoids the approximation to the dispersion relation that the Ginzburg–Landau model makes [Eq. (19)]. The linear coefficients τ_0 and ξ_0^2 occurring in (17) and used to predict threshold shifts in (26) are calculated on the basis of the Taylor expansion (19) to first order in ϵ and second order in k, valid only in the neighborhood of criticality, that is, near $\epsilon = 0$, $k = 0$. Numerically, we find that the quadratic approximation in k is valid only for very small k. Figure 3 shows for $\eta = 0.8703$ and $m = 3$ the numerically determined growth rate as a function of k within the first Brillouin zone $-\tau/\lambda_c < k < +\pi/\lambda_c$. The axial periodicity and reflection symmetry of the Taylor vortex base flow imply that ω is a periodic function of k with period $2\pi/\lambda_c$, and that $\partial_k \omega$ must be zero at the origin and at the zone boundaries. Thus the quadratic approximation must fail well before the zone boundary is reached. Also shown in the figure is a parabola fit to the numerical data at $k = 0$, which corresponds to the quadratic Ginzburg–Landau approximation.

To investigate the relevance of the two Floquet modes with $k = \pm \pi/L$, we conducted a numerical and experimental study of the onset of wavy vortices as a function of aspect ratio. The radius ratio 0.8703 was available in an existing experimental apparatus designed for another purpose,[10] and thus we chose to examine this case. We determined from linear calculations for the stability of Couette flow that the infinite-cylinder Taylor transition occurred at $R_c = 116.096$ with a critical wavelength $\lambda_c = 2.0076(b-a)$. Since it is well known that stable nonlinear Taylor vortices exist over a finite range of wavelengths, and since we did not wish to study the effect of Taylor vortex wavelength on the wavy

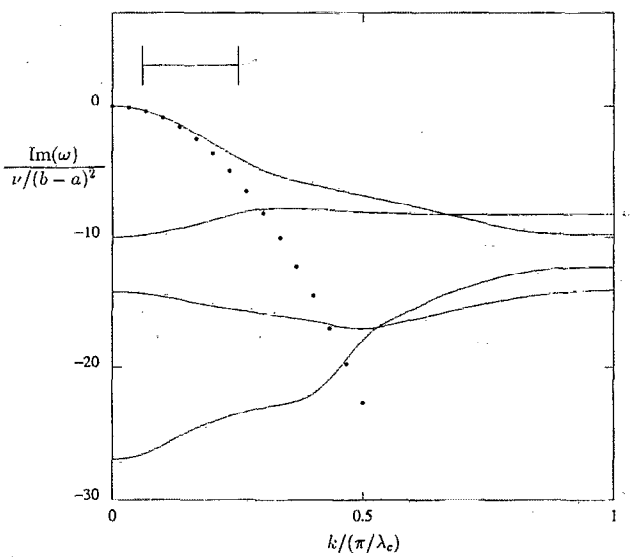

FIG. 3. Dispersion relation within the first Brillouin zone for parameters $\eta = 0.8703$, $\lambda_c = 2.0076$, $m = 3$, $R = 131.025$. The solid curves are growth rates of the four least stable modes. There is a countable infinity of more stable modes which are not shown. Only the leading mode, the one with maximum growth rate, is important for determining stability. The Reynolds number for this figure is critical for the onset of $m = 3$ waves, so that the leading eigenmode has $\mathrm{Im}(\omega) = 0$ for $k_W = 0$; this mode is associated with the uppermost solid curve. The dotted curve is a parabola fitted to the top curve at $k = 0$. The horizontal bar indicates the range of Floquet exponents $k = \pi/L$ explored in our numerical and experimental study for $L = 4\lambda_c$ to $17\lambda_c$. For this restricted range of Floquet exponents, the top curve does not intersect any other curve, so we may assume that only this mode is important.

transition, we chose to consider in both the numerics and experiment only those annulus lengths that are integer multiples of λ_c, that is, $L = L_n = n\lambda_c$, and we further insisted that in the experimental Taylor vortex flow for length L_n there were exactly n pairs of Taylor cells between the end rings. The end rings in the experiment were fixed, giving rise to Ekman pumping that results in end cells of slightly longer axial extent that those in the bulk of the column, which were then, of course, slightly shorter than λ_c; we will discuss this effect in a subsequent section when we analyze our experimental results.

The experimental apparatus had a maximum aspect ratio sufficient to accommodate 17 pairs of Taylor vortices. We studied the set of aspect ratios L_n, $n = 4,\ldots,17$. The horizontal bar in Fig. 3 covers the corresponding range of Floquet exponents $\pi/(17\lambda_c) \leqslant k \leqslant \pi/(4\lambda_c)$.

B. Computational protocol and results

Calculations of the critical Reynolds number R_W and azimuthal wave number m for the onset of waves in the infinite-cylinder case showed that the critical disturbance was an $m = 1$ wavy mode with $R_W = 126.68$. Calculations of threshold shifts, however, indicated that at the maximum achievable annulus length, $L = 17\lambda_c = 34.129(b-a)$, the $m = 1$ mode would be damped relative to $m = 3$, which would be the critical mode at that aspect ratio; that is, finite size suppresses $m = 1$. We began our computational procedure by finding the onset of the critical $m = 3$ mode for fixed Floquet exponent $k = \pi/(17\lambda_c)$. This yielded $R_W = 135.48$ with a frequency at onset of $\mathrm{Re}(\omega)/\Omega = 1.3754$. We checked that for the same Reynolds number and the same Floquet exponent, the modes $m = 2$ and $m = 4$ were damped relative to the neutral mode $m = 3$.

We then stepped down in aspect ratio, finding for each $k = \pi/(n\lambda_c)$, $n = 16,15,\ldots,4$ the critical Reynolds number and azimuthal wave number and then checking that the two adjacent azimuthal modes were damped. When we found that an adjacent azimuthal mode was not damped, we switched our attention to it, determined its critical Reynolds number, and then checked its neighboring azimuthal modes again. In this way the information in the numerical part of Table II was obtained.

In all cases we computed only the Floquet mode with $k = +\pi/(n\lambda_c)$ as the other, for $k = -\pi/(n\lambda_c)$, can be obtained trivially by reflection in z and the two are exactly degenerate.

Figure 4 shows the critical linear modes and Taylor vortex flow for the case $n = 10$. For clarity, Couette flow is omitted since otherwise it would completely dominate the velocity field. The overall helical form of the Floquet modes is apparent, as is the suppression of the wavy disturbances near the axisymmetric end boundaries when the two modes are superposed.

Our numerical method was not able to resolve the axisymmetric Taylor vortex flows for this radius ratio at Reynolds numbers in excess of approximately 1000. We found for $L = 3\lambda_c$ that azimuthal wave numbers $m = 7,8,9$ were damped up to this Reynolds number.

V. EXPERIMENTAL VERIFICATION

A. Description of the apparatus

We had available in our laboratory an apparatus designed and built by Hirst to study the aspect-ratio dependence of the attractor dimension in weak Couette–Taylor turbulence.[10] The system consisted of two independently rotating cylinders. The inner cylinder of brass was machined to a radius of $a = 6.635 \pm 0.005$ cm and the outer cylinder of precision bore glass tubing had an inner radius of $b = 7.620 \pm 0.005$ cm. For our study the outer cylinder was kept fixed. The cylinders were housed in a water bath which maintained the temperature at 24.5 °C to within 0.1 °C. The inner cylinder was driven by a computer-controlled microstepper motor through a system of timing belts and pulleys.

End boundary conditions were established by two nonrotating Teflon rings. The annulus length L was varied manually by moving one of these rings; L was measured to within 0.5 mm via a millimeter scale. The working fluid was a mixture of 65% glycerol, 34% water, and 1% Kalliroscope AQ-1000 flow visualization material. The kinematic viscosity of this mixture was approximately 0.1 $\mathrm{cm}^2/\mathrm{sec}$.

Frequency measurements were made by analyzing the light from a 10 mW helium–neon laser that was transmitted through the fluid along one of the Taylor vortex boundaries. The light entered through the outer cylinder at a small angle, passed along the outflow boundary, and exited through the outer cylinder. The transmitted light fell on a photodetector and the resulting intensity signal was digitized and then Fourier analyzed. The appearance of a time-periodic wavy flow resulted in sharp peaks in the power spectrum of this signal. Time-dependent waves of very small amplitude were detectable by this transmitted-light method.

B. Experimental protocol

For each of the lengths $L = L_n = n\lambda_c$, $n = 4,\ldots,17$, we set the movable end ring to the required position. We prepared a flow with n pairs of Taylor vortices by slowly increasing Ω (and thus R) through the Taylor transition; visual inspection confirmed the number of pairs. In a few cases it was necessary to shorten the annulus temporarily in order to obtain exactly n pairs; after the Taylor vortex pattern was established we then slowly increased L to the appropriate length; this procedure stretches the vortices due to a well known pinning of the phase of the pattern by the end rings. The value of R_W for transition to wavy vortices was then determined to within approximately one Reynolds number by manual motor speed adjustments and visual observations. Finally, a set of ten computer-controlled measurements were made at Reynolds number increments of 0.1; each measurement consisted of an adjustment to the motor speed, a 25 min settling time, and the recording of a digital time series from the photodetector. The transition Reynolds number R_W and wave frequency ω were determined from the appearance and location of peaks in the Fourier spectra of these time series.

The wavy transition occurred at much higher Reynolds numbers for the cases $n = 4$ and $n = 5$; here we used correspondingly larger Reynolds number increments of 0.5 and 0.2, respectively.

TABLE II. Numerical and experimental results for $\eta = 0.8703$. Experimental results are averages of the two sets of data; uncertainties in the last one or two digits are indicated by values in parentheses. See also Fig. 6.

L_n		Numerical				Experimental		
n	$n\lambda_c(b-a)$	R_W	m	$\mathrm{Re}(\omega)/\Omega$	$\mathrm{Im}(\omega)/\nu/(b-a)^2$	m	R_W	ω/Ω
4	8.030	527.77	7	2.5277	−0.6019	8	607(7)	2.840(13)
			8	2.9026	0.0000			
			9	3.2543	−1.2000			
5	10.038	202.12	7	2.8255	−0.1441	8	209(7)	3.25(9)
			8	3.1992	0.0000			
			9	3.5638	−0.7559			
6	12.046	177.30	6	2.5057	−0.0423	7	178.8(5)	2.909(13)
			7	2.8918	0.0000			
			8	3.2701	−0.6685			
7	14.053	164.37	5	2.1451	−0.1012	6	164.7(5)	2.555(13)
			6	2.5454	0.0000			
			7	2.9377	−0.5309			
8	16.061	155.99	4	1.7554	−0.2681	5	156.0(10)	2.174(6)
			5	2.1705	0.0000			
			6	2.5775	−0.3123			
9	18.068	151.33	4	1.7668	−0.0225	5	151.5(5)	2.197(8)
			5	2.1868	0.0000			
			6	2.5983	−0.5602			
10	20.076	146.69	3	1.3476	−0.2906	4	146.7(5)	1.782(8)
			4	1.7806	0.0000			
			5	2.2058	−0.2092			
11	22.084	143.82	3	1.3537	−0.1491	4	144.2(8)	1.792(5)
			4	1.7899	0.0000			
			5	2.2187	−0.3600			
12	24.091	141.98	3	1.3578	−0.0533	4	141.8(6)	1.798(8)
			4	1.7962	0.0000			
			5	2.2276	−0.4614			
13	26.099	140.38	2	0.9138	−0.3132	4	140(3)	1.802(10)
			3	1.3617	0.0000			
			4	1.8021	−0.0293			
14	28.106	138.52	2	0.9169	−0.2364	3	138.6(10)	1.365(6)
			3	1.3667	0.0000			
			4	1.8097	−0.1213			
15	30.114	137.20	2	0.9191	−0.1795	3	137.1(5)	1.372(5)
			3	1.3704	0.0000			
			4	1.8152	−0.1886			
16	32.122	136.23	2	0.9209	−0.1356	3	135.6(5)	1.372(6)
			3	1.3732	0.0000			
			4	1.8194	−0.2396			
17	34.129	135.48	2	0.9222	−0.1008	3	134.7(5)	1.374(5)
			3	1.3754	0.0000			
			4	1.8227	−0.2796			

We obtained two complete sets $n = 4,\ldots,17$ of measurements; after the first set the inner cylinder was painted black and a new batch of working fluid was introduced. The black paint increased the radius ratio from $\eta = 0.8703$ to $\eta = 0.8708$. For the second set of measurements the Reynolds number increments were 0.12, except as noted for $n = 4,5$. Figure 5 is a photograph of the observed wavy vortex flow for $n = 9$.

C. Experimental errors

Experimental uncertainty in viscosity, typically 2% or greater, exceeds other purely mechanical uncertainties such as the tolerances associated with fabrication of the cylinders, the error in the motor speed, and the error in placement of the movable end ring. For this reason we scaled the wave frequency by the inner cylinder speed at onset of the wave,

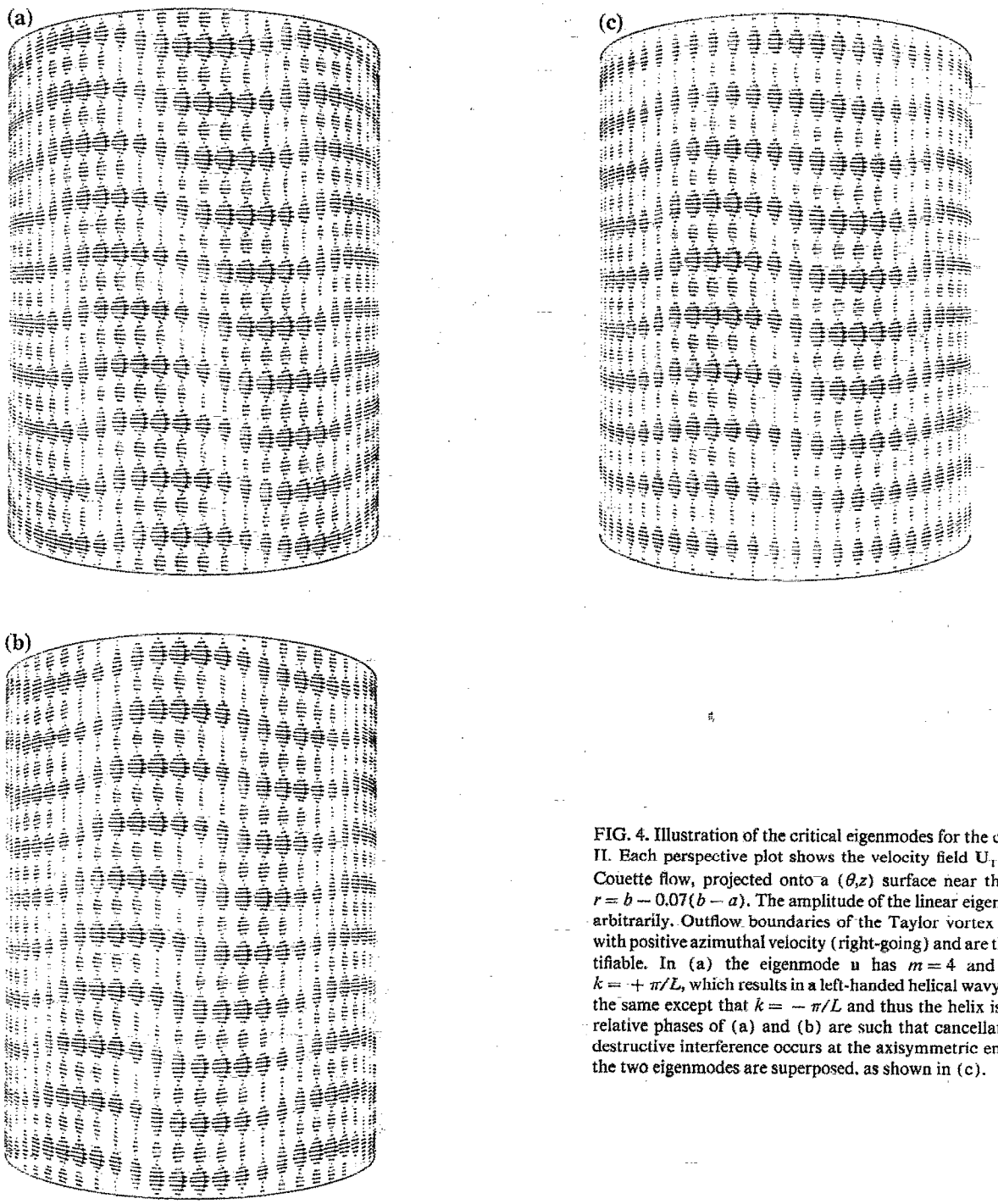

FIG. 4. Illustration of the critical eigenmodes for the case $n = 10$ of Table II. Each perspective plot shows the velocity field $\mathbf{U}_T + \mathbf{u}$, not including Couette flow, projected onto a (θ,z) surface near the outer cylinder at $r = b - 0.07(b-a)$. The amplitude of the linear eigenmode $\mathbf{u}$ was chosen arbitrarily. Outflow boundaries of the Taylor vortex flow are correlated with positive azimuthal velocity (right-going) and are therefore easily identifiable. In (a) the eigenmode $\mathbf{u}$ has $m = 4$ and Floquet exponent $k = +\pi/L$, which results in a left-handed helical wavy pattern. Part (b) is the same except that $k = -\pi/L$ and thus the helix is right-handed. The relative phases of (a) and (b) are such that cancellation of the wave by destructive interference occurs at the axisymmetric end boundaries when the two eigenmodes are superposed, as shown in (c).

since the ratio ω_W/Ω_W is viscosity independent. We obtained the viscosities by assuming that the Taylor transition took place at $R_c = 116.096$, as predicted by infinite-cylinder linear stability calculations. However, experimental determination of the Taylor transition is highly subjective due to Ekman pumping at the ends. Therefore, for each of the two sets $n = 4,...,17$ of measured onset Reynolds numbers R_W, we assumed that a single value of the viscosity applied to the entire set, *and this value was chosen to fit the theoretical results from Table II.* The measured viscosities based on the Taylor transitions were 0.099 and 0.094 cm^2/sec for the two batches of fluid, while the fitted viscosities were 0.100 and 0.096 cm^2/sec, respectively.

D. Flow features at low aspect ratios

We also experimentally investigated the flow at $L = 2\lambda_c$ and $L = 3\lambda_c$. In both cases transition occurred at Reynolds numbers in excess of 1500. The first nonaxisymmetric flow pattern had a high azimuthal wave number and an appearance similar to the twist vortices reported, for example, by Andereck *et al.*[11] At higher Reynolds numbers the twists

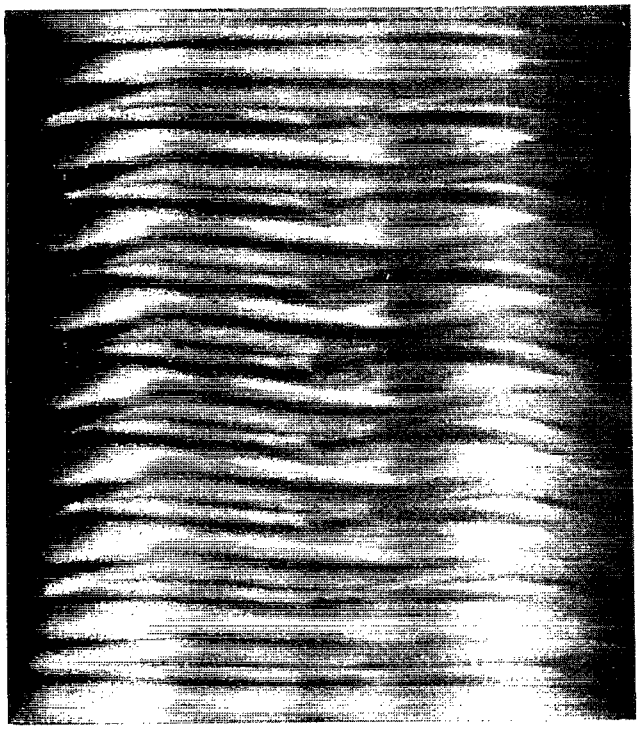

FIG. 5. Photograph of the experimental $m = 5$ wavy flow near onset for the case $n = 9$ of Table II. The suppression of the wavy disturbance near the axisymmetric end rings is evident. Compare Fig. 4(c).

started pulsing, that is, appearing and disappearing very quickly at a frequency of about once every two inner cylinder periods. At still higher Reynolds numbers the boundaries of these vortices developed waves.

VI. COMPARISON OF THEORETICAL AND EXPERIMENTAL RESULTS

A. Quantitative comparison

Table II and Fig. 6 compare the results of the linear stability calculations and experiment for annulus lengths $L = 4_c,...,17\lambda_c$. The critical azimuthal wave number is correctly predicted in all cases except $n = 13$, where $m = 3$ is predicted and $m = 4$ is observed. This anomaly is as yet unexplained; we note, however, that for this case the $m = 4$ mode was found numerically to be only slightly damped (growth rate $\mathrm{Im}(\omega)/[\nu/(b-a)^2] = -0.0293$); a similar situation occurs for $m = 4$ at $n = 9$ (growth rate -0.0225) but does not result in an incorrect prediction. The experimental wave frequencies agree in all cases to within experimental error, with the exception of $n = 13$ where the frequency agrees with the computed $m = 4$ frequency, and the case $n = 4$ where the experimental wave frequency is 2% lower than the predicted value. Reynolds numbers at onset, after adjustment of the viscosity of each batch of working fluid as previously discussed, agree well with computed critical Reynolds numbers except at very low aspect ratios where the experimental numbers are several percent higher.

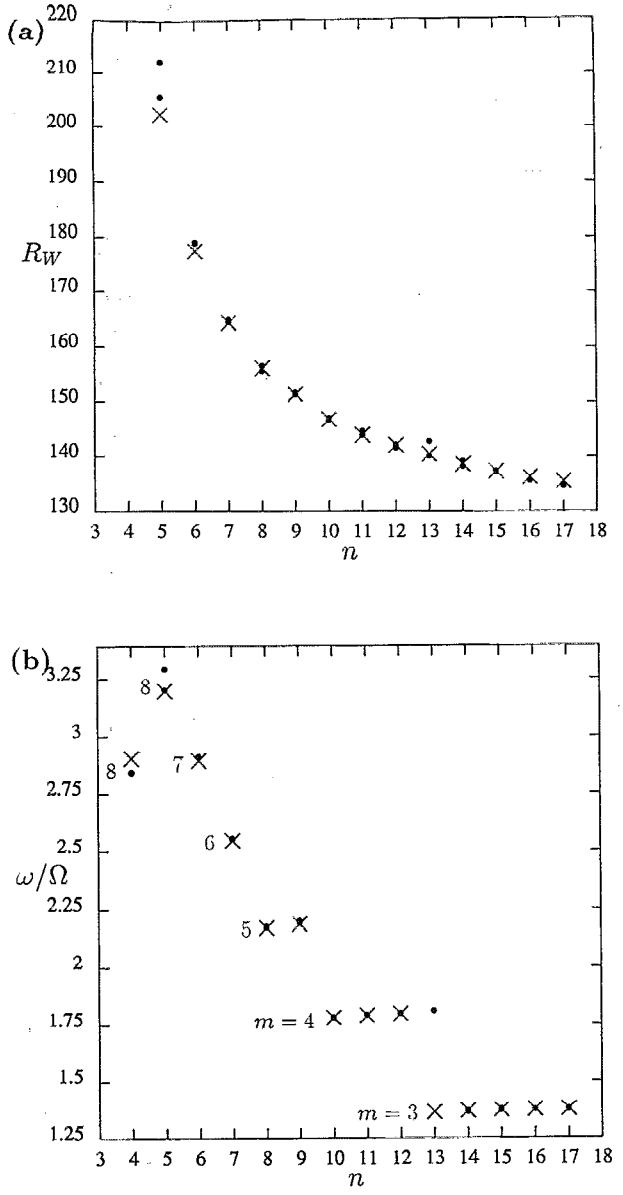

FIG. 6. Comparison of theoretical and experimental Reynolds numbers (a) and wave frequencies (b) at onset, from Table II, for annulus lengths $L_n = n\lambda_c$. Theoretical values are indicated by crosses. For each value of n there are two experimental points shown as solid dots; the two dots are in most cases indistinguishable on these scales. In (a) the case $n = 4$ is omitted; see Table II for these values of R_W. In (b) the results are clearly grouped by the azimuthal wave numbers shown; for example, the five points at lower right are for $m = 3$. Note the disagreement in azimuthal wave number for $n = 13$; in all other cases the predicted and observed azimuthal wave numbers agree.

B. Ekman-pumped end vortices

It is well known that fixed end rings in experiments affect the adjacent Taylor vortices as a result of Ekman pumping. The phase of the pattern is pinned such that the flow in the boundary layer adjacent to each end ring has an inward radial component; the first genuine vortex boundary away from the ends is thus an outflow boundary. As previously

noted, we sometimes used this pinning effect to prepare Taylor vortex flows with a desired number n of vortex pairs in an annulus of length $L = n\lambda_c$. Ekman pumping also results in end vortices of slightly larger axial extent than those in the bulk of the column. We attempted in a few cases to correct for this latter effect by adjusting the length of the annulus until the vortices in the bulk were of axial length λ_c as measured by a traveling telescope. At long aspect ratios the effect of this adjustment was less than 0.5% in the scaled onset frequencies. At shorter aspect ratios the onset Reynolds number became very sensitive to small adjustments, for example, changing by 15% for a 3% length adjustment. The values in Table II and Fig. 6 are for $L = L_n = n\lambda_c$ without compensation for the Ekman-pumped end cells.

VII. CONCLUSIONS

We have studied the general linear problem for the stability of Taylor vortices with respect to arbitrary disturbances, with special emphasis on the Floquet exponent k and the relevance of certain Floquet modes to the problem of the onset of wavy vortices in finite-length systems. Our numerical calculations have provided independent values for the linear coefficients of Ginzburg–Landau equations which have been compared with previous experimental results. We have examined the dispersion relation $\omega = \omega(m,k;\epsilon)$ for k within the first Brillouin zone defined by the spatially periodic Taylor vortex flow. We find that the quadratic approximation to this dispersion relation near $k = 0$ deviates significantly from the actual dispersion relation when k is of the order of $\pi/15\lambda_c$. This suggests that the first eigenmode of the Ginzburg–Landau equation, used to predict threshold shifts, will not be reliable for aspect ratios of approximately 30 and below.

For aspect ratios between $4\lambda_c \approx 8$ and $17\lambda_c \approx 34$ we have conducted a detailed numerical and experimental study which indicates that the onset of wavy vortices may be accurately predicted by assuming that the finite-cylinder eigenmode is the superposition of two infinite-cylinder Floquet modes with $k = \pm \pi/L$. We know of no other theoretical model in which critical Reynolds numbers, azimuthal wave numbers, and wave speeds of wavy vortices agree in detail with experiment over this range of aspect ratios.

Although our work is computationally more intensive than perturbation analyses such as that of Walgraef *et al.*[9] or infinite-cylinder stability calculations such as those of Jones,[3,4] it is important to note that our calculations were all performed on a small two-dimensional (r,z) domain, periodic in z with period λ_c. No attempt was made to accurately model the actual end boundary conditions in finite-length experiments. We conclude that the detailed flow features near the ends are largely irrelevant to the problem of transition to wavy vortices over the range of aspect ratios we have studied, and that the only important effect of the axisymmetric boundaries is the localized suppression of the nonaxisymmetric disturbance.

Having successfully modeled the linear problem in terms of two discrete Floquet modes $k = \pm \pi/L$, we speculate that the weakly nonlinear behavior of wavy vortices might also be studied by an approximation scheme in which the velocity field is expanded in a small number of modes with $k = k_q = q\pi/L$ for integers q. The intermediate aspect ratios we have studied in this paper might be productively investigated via relatively simple nonlinear models involving a small number of discrete modes.

ACKNOWLEDGMENTS

The authors wish to thank Randy Tagg and Austin Holiday for their help with the experiments, and Laurette Tuckerman, Richard Friesner, and Dan Sorensen for valuable discussions and for the use of their computer codes. Harry Swinney read the manuscript thoroughly and his suggestions have substantially improved it. We appreciated the very careful design and construction of Don Hirst's apparatus which expedited the experimental work. We also thank the referees for several very valuable suggestions that have improved both the content and organization of the paper.

This research is supported in part by the Office of Naval Research Nonlinear Dynamics Program, and by NSF Grant No. DMS-8901767. Computational resources for this work were provided by the University of Texas System Center for High Performance Computing.

[1] G. I. Taylor, Philos. Trans. R. Soc. London Ser. **223**, 289 (1923).
[2] J. A. Cole, J. Fluid Mech. **75**, 1 (1976).
[3] C. A. Jones, J. Fluid Mech. **102**, 249 (1981).
[4] C. A. Jones, J. Comput. Phys. **61**, 321 (1985).
[5] M. A. Dominguez-Lerma, G. Ahlers, and D. S. Cannell (unpublished).
[6] G. Pfister and I. Rehberg, Phys. Lett. A **83**, 19 (1981).
[7] G. Ahlers, in *Lectures in the Sciences of Complexity, SFI Studies in the Sciences of Complexity*, edited by D. Stein (Addison–Wesley, Reading, MA, 1989), pp. 175–224.
[8] W. S. Edwards, L. S. Tuckerman, R. A. Friesner, and D. C. Sorensen (in preparation).
[9] D. Walgraef, P. Borckmans, and G. Dewel, Phys. Rev. A **29**, 1514 (1984).
[10] D. A Hirst, Ph.D. thesis, University of Texas, 1987.
[11] C. D. Andereck, S. S. Liu, and H. L. Swinney, J. Fluid Mech. **164**, 155 (1986).